

On the Structural Sensitivity of Deep Convolutional Networks to the Directions of Fourier Basis Functions

Yusuke Tsuzuku
The University of Tokyo
RIKEN
tsuzuku@ms.k.u-tokyo.ac.jp

Issei Sato
The University of Tokyo
RIKEN
sato@k.u-tokyo.ac.jp

Abstract

Data-agnostic quasi-imperceptible perturbations on inputs can severely degrade recognition accuracy of deep convolutional networks. This indicates some structural instability of their predictions and poses a potential security threat. However, characterization of the shared directions of such harmful perturbations remains unknown if they exist, which makes it difficult to address the security threat and performance degradation. Our primal finding is that convolutional networks are sensitive to the directions of Fourier basis functions. We derived the property by specializing a hypothesis of the cause of the sensitivity, known as the linearity of neural networks, to convolutional networks and empirically validated it. As a by-product of the analysis, we propose a fast algorithm to create shift-invariant universal adversarial perturbations available in black-box settings.

1 Introduction

Malicious perturbations on inputs can easily change predictions of deep learning models [33]. These perturbations are called adversarial perturbations or adversarial examples. They have been intensively studied in deep convolutional networks for object recognition tasks [33, 6, 19, 23, 3]. They are attracting attentions because they are potential security threat, and at the same time, expected to reveal some structural tendency of machine learning models. One of the intriguing aspects of adversarial perturbations is their universality. Szegedy et al. [33] observed transferability of the perturbations between classifiers. Papernot et al. [28] exploited the transferability to attack black-box models. Some adversarial perturbations transfer not only between



Figure 1: Examples of images perturbed by single Fourier attack. Added perturbation is the same as in Figure 3. The size of perturbations is $10/255$ in ℓ_∞ -distance for the first row and $20/255$ for the second. We see in Sec. 5.7 that the single $10/255$ and $20/255$ perturbations could change predictions for around 40% and 70% of inputs for various architectures, respectively.

classifiers but also between inputs. Goodfellow et al. [6] first discovered the universality, and Moosavi-Dezfooli et al. [24] studied this phenomenon in more detail. They found that a single perturbation can change models' predictions for a significant portion of data points. Such input-agnostic perturbations are called universal adversarial perturbations (UAPs). The perturbations also generalize between different networks to some extent. Figure 2 shows examples of UAPs calculated by Moosavi-Dezfooli et al. [24]. The existence of UAPs suggests some structural weakness of current models, especially of deep convolutional networks. Eliminating the weakness will enhance accuracy, robustness, and reliability of models. To achieve this goal, we first need to better understand the universal instability.

Several prior studies tried to understand the properties of the universality and transferability. Goodfellow et al. [6] explained the existence of adversarial examples, their transferability, and their universality using linearity of deep neural networks. Tramèr

et al. [35] investigated the transferable subspace of adversarial perturbations and suggested that it will consist of a high-dimensional continuous subspace. Moosavi-Dezfooli et al. [25] showed that the existence of universal adversarial perturbations is inevitable given strong geometrical assumptions on the decision boundary of models.

Given the transferability and universality of adversarial perturbations, it is natural to expect the existence of a set of directions that most networks are input-agnostically sensitive to. If we can characterize such directions, it enables us to improve robustness against such perturbations in systematic manners. However, prior studies are only able to create such perturbations by sequential optimizations, lacking useful characterizations of them. We provide the missing characterization of the directions by an analysis through Fourier basis. The motivation of the analysis comes from two parts. The first is the linear hypothesis of vulnerability, and the second is a property of linear convolutional layers that the singular vectors are Fourier basis functions. The property indicates that sensitive directions of convolutional networks are a combination of a few Fourier basis functions. Through extensive experiments on various architectures and datasets, we found networks are sensitive to Fourier basis functions of some specific frequencies. In other words, we could characterize at least a subset of universal and transferable adversarial perturbations through Fourier basis. We also observed that some adversarial perturbations exploits the sensitivity to Fourier basis functions. These findings not only provide new characterization of adversarial perturbations, but also suggest a possibility that some known properties of the universality of adversarial perturbations might be due to the structure of convolutional networks. As a by-product of our analysis, we developed a fast method to create shift-invariant universal adversarial perturbations, which is available in black-box settings. Figure 1 shows examples of perturbed images created by our algorithm, which is explained in Sec. 4. Our perturbations have simple and shift-invariant patterns, yet achieved high fool ratio on various pairs of architectures and datasets.

Our contributions are summarized below.

1. We characterized transferable and universal directions of adversarial perturbations using Fourier basis.
2. We evaluated our hypothesis in extensive experiments.
3. We proposed a fast black-box algorithm to create shift-invariant universal adversarial perturbations.

2 Related work

2.1 Adversarial perturbations

One of the most famous adversarial perturbations creation algorithms is the fast gradient sign method (FGSM) [6]. Let $J(\theta, x, t)$ be a loss with parameter θ , an input x , and a target label t . Then, FGSM uses $\epsilon \cdot \text{Sign}(\nabla_x J(\theta, x, t))$ as the perturbation, where ϵ is a scaling parameter. Another popular approach is performing gradient ascent on some



Figure 2: Examples of images perturbed by universal adversarial perturbations calculated by Moosavi-Dezfooli et al. [24].

loss $J(\theta, x, t)$. Depending on the choice of the loss and the optimization methods, there are numerous variants for attacks [3, 23].

Adversarial training [6] is a current effective countermeasure against adversarial perturbations. Kurakin et al. [19] conducted a large-scale study on adversarial training, and Tramèr et al. [36] extensively studied the transferability for defended and undefended models.

Evaluations of defense methods are notoriously difficult [2, 37]. Thus, some studies have provided theoretically grounded defense methods [16, 38].

2.2 Universal adversarial perturbations

Moosavi-Dezfooli et al. [24] showed that some input-independent perturbations can significantly degrade classifiers’ prediction accuracy. Such perturbations are called universal adversarial perturbations (UAPs). We define fool ratio as the ratio of the change of predictions. For a subset of training data X , we sequentially create adversarial perturbations until we achieve desired fool ratio. To create UAPs, we do not need access to test data. Moosavi-Dezfooli et al. [24] showed that UAPs can change over 80% of the predictions of various networks trained on ILSVRC2012 [29]. Figure 2 shows examples of UAPs created by Moosavi-Dezfooli et al. [24].

UAPs also generalize between network architectures to some extent. Recently, Mopuri et al. [26] and Khrulkov and Oseledets [15] proposed activation-maximization approaches for the creation of UAPs.

2.3 Analysis of transferability and universality

Goodfellow et al. [6] explained the existence of adversarial examples, their transferability, and their universality by linear hypothesis. In their explanation, since neural networks are too linear, directions are most important in adversarial examples. Thus, adversarial perturbations generalize between clean examples. Transferability is explained by the following two factors: (1) adversarial perturbations are aligned with the weight vectors of models, (2) different models learn similar functions. Tramèr et al. [35] analyzed the dimensionality of the subspace that adversarial examples lie in. Using first-order approximation, they found that adversarial examples lie in a high-dimensional subspace, suggesting overlap of the subspace between classifiers. However, the structure of the subspace is unknown except for its estimated dimensionality.

Liu et al. [22] observed that targeted attack is harder to transfer than an untargeted one. Moosavi-Dezfooli et al. [25] analyzed the existence of UAPs using strong geometrical assumptions. They also proposed an algorithm to find UAPs using Hessian on input, while it is prohibitively slow with large inputs.

We explain the existence of UAPs on the basis of the linear hypothesis of Goodfellow et al. [6]. We push forward the analysis concerning convolutional networks.

2.4 Fourier basis

Jo and Bengio [13] examined whether CNNs learn high-level features by using Fourier features. Some prior work used JPEG compression or other transformations to remove high-frequency features from images as a defense against adversarial examples [14, 8, 32]. However, connections to universality have not been explored. We also note that our experiments show that adversarial perturbations do not necessarily lie in high-frequency spots.

3 Preliminary and notation

In this section, we describe the relationship between convolutional layers and Fourier basis.

3.1 Circulant matrix

Let c be a vector and c_i be the i -th element of the vector c . A circulant matrix is a matrix with the following shape.

$$\text{Circ}(c_{\cdot}) = \begin{bmatrix} c_0 & c_1 & \dots & c_{n-2} & c_{n-1} \\ c_1 & c_0 & c_1 & & c_{n-2} \\ \vdots & c_{n-1} & c_0 & \ddots & \vdots \\ c_2 & & \ddots & \ddots & c_1 \\ c_1 & c_2 & \dots & c_{n-1} & c_0 \end{bmatrix}.$$

A doubly block circulant matrix is a block matrix whose blocks are circulant. The matrix A below is an example of a doubly block circulant matrix.

$$A = \begin{bmatrix} \text{Circ}(K_{0,\cdot}) & \text{Circ}(K_{1,\cdot}) & \dots & \text{Circ}(K_{n-1,\cdot}) \\ \text{Circ}(K_{n-1,\cdot}) & \text{Circ}(K_{0,\cdot}) & & \text{Circ}(K_{n-2,\cdot}) \\ \vdots & \text{Circ}(K_{n-1,\cdot}) & \ddots & \vdots \\ \text{Circ}(K_{2,\cdot}) & & \ddots & \text{Circ}(K_{1,\cdot}) \\ \text{Circ}(K_{1,\cdot}) & \text{Circ}(K_{2,\cdot}) & \dots & \text{Circ}(K_{0,\cdot}) \end{bmatrix},$$

where $K_{i,\cdot}$ is a i -th row of a matrix K . When the channel size of a convolutional layer is equal to one and padding is “wraps around,” convolution operation can be written as a doubly block circulant matrix [5, 30]. We later describe a case where channel size is larger than one.

3.2 Fourier basis and discrete Fourier transformation

Let us define $\omega_N^{i,j} = \omega_N^i \omega_N^j \in \mathbb{C}^{N \times N}$, where $\omega_N = \exp(2\pi\sqrt{-1}/N)$ is the N -th root of an imaginary number. We define F_N be a matrix such that the (i, j) -th element is $(F_N)_{i,j} = \omega_N^{i,j}$. We notate the i -th row of F_N as $(F_N)_i$. Let us define transformation $S : \mathbb{C}^{N \times N} \rightarrow \mathbb{C}^{N \times N}$ as follows.

$$S(x) = \sum_{m=0}^N \sum_{n=0}^N x_{m,n} \exp(-2\pi i(um + vn)/N).$$

This transformation S is called discrete Fourier transformation (DFT). Both the transformation and its inverse can be calculated in the running time of $O(N \log N)$ by using fast Fourier transformation [4].

3.3 Decomposition of convolution operator

We define $Q := \frac{1}{N} F_N \otimes F_N$. The eigenvectors of a doubly block circulant matrix are known to be Q [11]. Since Q is unitary, a doubly block circulant matrix can be decomposed as QDQ^H , where Q^H is an adjoint matrix of Q and D is a complex diagonal matrix. In a case where channel size is one, since convolution is a doubly circulant matrix, the above analysis is directly applicable. Now, we describe the situation where input-output channel size is $m \geq 1$, and the width and height of the input is N . Let R be $I_m \otimes Q$ and L be some $N^2 m \times N^2 m$ block matrix such that each matrix is an $N^2 \times N^2$ complex diagonal matrix. Then, using R and some L , the convolution operator can be written as RLR^H [30]. Extending this result to the cases where input and output channel sizes are different is straightforward.

4 Fourier analysis

In this section, we show that the most sensitive direction of linear convolutional networks is a combination of a few Fourier basis functions. This pushes forward the linear hypothesis of the cause of adversarial examples in Goodfellow et al. [6]. The linear approximation may not hold well for deep non-linear networks. However, we can still expect that adding some Fourier basis to input largely disturbs hidden representations of networks.

4.1 Sensitivity of stacked convolution

We first consider stacked stride-1 convolutional layers without activation functions, with m_1 input channels and m_2 output channels. From Sec. 3.3, the i -th convolutional layer can be written as $RL_i R^H$. Since R is unitary, the network can be written as $R(\prod_i L_i) R^H$. Let us consider a $m_1 \times m_2 \times N \times N$ tensor G composed of non-zero elements of $L := \prod_i L_i$ as follows: $G_{cdw_1w_2} = (L_{cd})_{w_1w_2}$, where L_{cd} is a (c, d) -th block of L . Let x be a singular vector of $G_{:, :, w_1, w_2}$; then $x \otimes (F_N)_{w_1} \otimes (F_N)_{w_2}$ is a singular vector of RLR^H [30]. Since all singular vectors of RLR^H can be written in the form $x \otimes (F_N)_{w_1} \otimes (F_N)_{w_2}$. This means the most sensitive direction of the

stacked convolutional layers is a linear combination of a single Fourier basis functions between input channels. Thus, manipulating a single Fourier basis on inputs is the most effective way to disturb the prediction of the network. This analysis also holds when batch-normalization layers and skip connections exist.

4.2 Reduction layers

We first consider stride-2 convolutions. The stride-2 convolution can be decomposed into stride-1 convolution and subsampling of its output. Let the output of the stride-1 convolution be $x := \sum_i^N \sum_j^N \lambda_{i,j} (F_N)_i \otimes (F_N)_j$. Since the subsampling maps $(F_N)_i \otimes (F_N)_j$ to $(F_{N/2})_i \otimes (F_{N/2})_j$, the output of the subsampling y is

$$\sum_i^{N/2} \sum_j^{N/2} (\lambda_{i,j} + \lambda_{i+\frac{N}{2},j} + \lambda_{i,j+\frac{N}{2}} + \lambda_{i+\frac{N}{2},j+\frac{N}{2}}) (F_{\frac{N}{2}})_i \otimes (F_{\frac{N}{2}})_j.$$

Thus, at reduction layers, there are interactions between frequencies even under the linear approximation. However, the type of mixing is still limited, and we can still write the most sensitive direction of networks by a combination of a few Fourier basis functions. Extending this analysis to other sizes of strides and average poolings is straightforward.

4.3 Single Fourier attack

We propose an algorithm to find universal adversarial perturbations using Fourier basis. The attack exploits the sensitivity of convolutional networks to the Fourier basis directions analyzed in the previous section. The algorithm is as follows: we select one Fourier basis function and use it as a perturbation. However, this is incompatible with the restriction that the input must be real. Since $S(x)_{i,j} = S(x)_{N-i,N-j}^*$, where $S(x)^*$ is a conjugate, for real input x and vice versa, we make $S(x)_{i,j} = S(x)_{N-i,N-j}^*$ satisfied to keep the real-value constraint. Algorithm 1 shows the pseudocode of the algorithm, which is named single Fourier attack (SFA). Figure 3 shows a visualization of Fourier basis in 8×8 space and an example of perturbations created by SFA. Figure 1 shows examples of perturbed images. We can see that this attack does not change human’s predictions, and models should be robust against this. Discrete cosine transformation [1] is another way to avoid having complex values appear. In this paper, however, we use only the original Fourier basis functions to keep the connection to Fourier basis clearer. The method to select which Fourier basis functions to use is described in Sec. 5.2 and Sec. 5.7. We note that the method does not require gradients nor logits of target model, and hence available in black-box settings.

5 Experiments

We presented a characterization of the adversarial directions through Fourier basis in Sec. 4. To show that the characterization well describes the nature of the adversarial directions, we conducted a series of experiments. Primarily, we answer the following questions.

Algorithm 1: Single Fourier attack

hyperparam: i, j : frequency, ϵ : size of perturbation

input : x : image

foreach c in channel:

$x_c \leftarrow x_c + \epsilon((1+i)(F_N)_i \otimes (F_N)_j$
 $+ (1-i)(F_N)_{N-i} \otimes (F_N)_{N-j});$

$x_c \leftarrow \text{Clip}(x_c, 0, 1);$

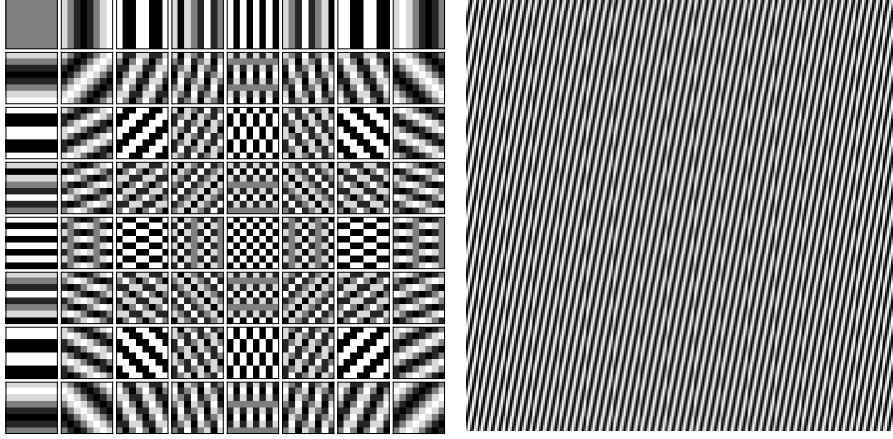


Figure 3: Left: Visualization of Fourier basis in 8×8 space. Row i and column j shows $(F_8)_i \otimes (F_8)_j$. Right: An example of perturbations created by Single Fourier attack in Alg. 1.

1. Whether Fourier basis characterization is better than others such as pixel basis (Sec. 5.2).
2. Whether the sensitivity to the Fourier basis directions is unique to convolutional networks (Sec. 5.3).
3. Whether UAPs are related to Fourier basis directions (Sec. 5.5).
4. Whether current white-box attacks are also related to Fourier basis directions (Sec 5.6).
5. Whether manipulation on a single Fourier basis can image-agnostically change predictions of various convolutional networks (Sec. 5.7).

In the following experiments, we affirmatively answer the above questions.

5.1 Evaluation setup

Datasets: We used as datasets MNIST [21], fashion-MNIST [39], SVHN [27], CIFAR10, CIFAR100 [17], and ILSVRC2015 [29]. For training on CIFAR10 and CI-

FAR100, we augmented data with padding with four followed by random crop and horizontal flip. We then normalized them with the mean and std of each channel. For training on ILSVRC2015, we rescaled images with its shorter side randomly sampled in $[256, 480]$ and randomly cropped into 224×244 for scale augmentation [31]. We used per-channel subtraction and standard color augmentation [18]. For other datasets, we scaled inputs into the range from zero to one.

Architectures: We used a multi-layer perceptron (MLP) consisting of 1000–1000 hidden layer with ReLU activation, LeNet [20], WideResNet [40], DenseNet-BC [10], and VGG [31] with batch-normalization for evaluations on datasets except for ILSVRC2015. For ILSVRC2015, we used ResNet50 [9], DenseNet, VGG16, and GoogLeNet [34]. For VGG16 and GoogLeNet, we added a batch-normalization layer after each convolution for faster training.

Training details except for ILSVRC2015: We used Nesterov momentum as an optimizer with momentum 0.9, weight decay 0.0005, and batchsize 128 for the experiments. We trained the MLP and LeNet for 50 epochs with an initial learning rate 0.1 decayed by 0.1 at every 10 epochs. We trained WideResNet as follows. For MNIST, fashion-MNIST, and SVHN, we used width factor $k = 4$, layer 16, and dropout ratio 0.4, and trained for 160 epochs with initial learning ratio 0.01 decayed by 0.1 at epoch 80 and 120. For CIFAR10 and CIFAR100, we used width factor $k = 10$, layer 28, and dropout ratio 0.3, and trained for 200 epochs with initial learning ratio 0.1 decayed by 0.1 at epoch 60, 120, and 160. These are the same configuration for SVHN and CIFAR in Zagoruyko and Komodakis [40]. We trained DenseNet-BC with layer 100, growth rate 12, and dropout ratio 0.2.

Training details on ILSVRC2015: We used SGD with momentum 0.9, weight decay 0.0001, and batchsize 256, and trained for 90 epochs for all architectures. For ResNet50, GoogLeNet, and VGG16, we used the same learning rate scheduling and momentum correction used by Goyal et al. [7]. For DenseNet121, we set an initial learning rate to 0.1 and multiplied by 0.1 at epoch 30 and 60, following Huang et al. [10].

Metric: We use as a metric the fool ratio, which is the percentage of data that models changed its prediction, following Moosavi-Dezfooli et al. [24].

5.2 Fourier domain vs pixel domain

We analyzed the sensitivity of the deep convolutional networks to Fourier basis directions in Sec. 4. To validate the analysis, we investigated the sensitivity on each Fourier basis. For comparison, we checked sensitivity against manipulation on each pixel. We also tested sensitivity in random directions (see Sec. 5.7). We first describe the method we used to study the sensitivity. For Fourier basis, we applied single Fourier attack (Algorithm. 1) and calculated its fool ratio on a single minibatch for each frequency. We bounded the size of perturbations by $30/255$ in ℓ_∞ -norm for MNIST, FMNIST, and

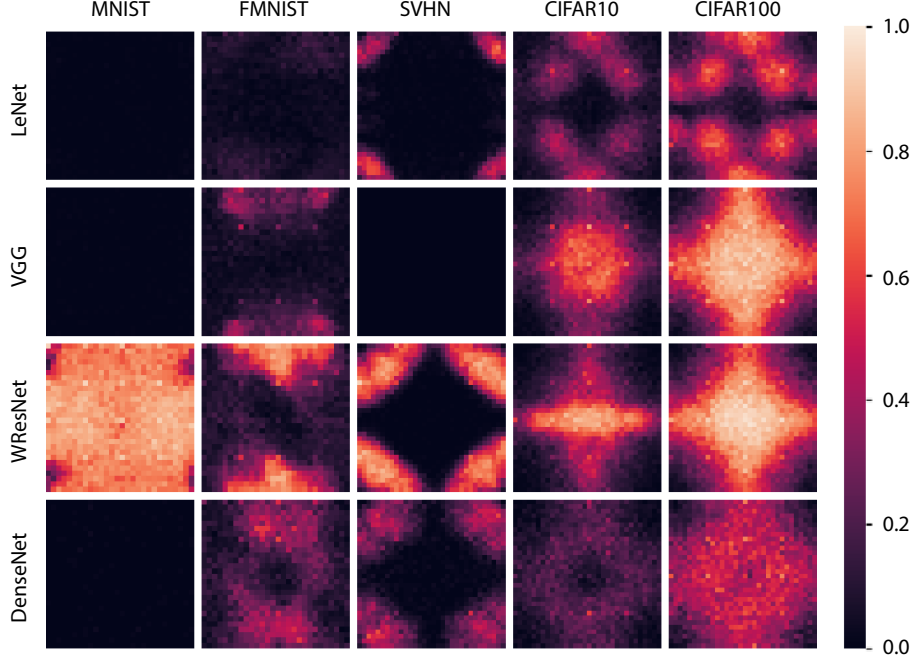


Figure 4: Visualization of sensitive spot of convolutional networks in the Fourier domain. Coordinate (i, j) of each image represents fool ratio on a single minibatch when we used Algorithm 1 as a perturbation. White areas are spots with high fool ratio. The center of each image corresponds to a high-frequency area. The perturbation sizes were 30/255 for MNIST, FMNIST, and SVHN, and 10/255 for CIFAR10 and CIFAR100.

SVHN, 20/255 for ILSVRC2015, and 10/255 for CIFAR10 and CIFAR100. For pixel basis, we added 255/255 to each pixel and then clipped to range from zero to one for attack creation, which is an analogy of Algorithm 1. Using heat maps, we visualized the results for Fourier basis on ILSVRC2015 in Figure 5 and the results on the other datasets in Figure 4. We observed that in most cases except for MNIST, architectures tend to have some sensitive spots in the Fourier domain. Especially on CIFAR10 and CIFAR100, VGG and Wide-ResNet showed near 90% and 99% fooling ratio to some directions. This means the predictions became almost random guess. Since all vectors in Fourier basis are orthogonal, Figure 4 highlights that there are hundreds of directions that networks are weak independent of their inputs. While it has been known that there are tens of orthogonal directions for transferable or universal adversarial examples, to the best of our knowledge, this is the fastest method to find a large number of orthogonal directions that networks are universally vulnerable for. Contrastive to Fourier basis, experiments in pixel basis achieved almost 0% fool ratio in all settings. In this experiment, we showed the existence of sensitive spots of convolutional networks in

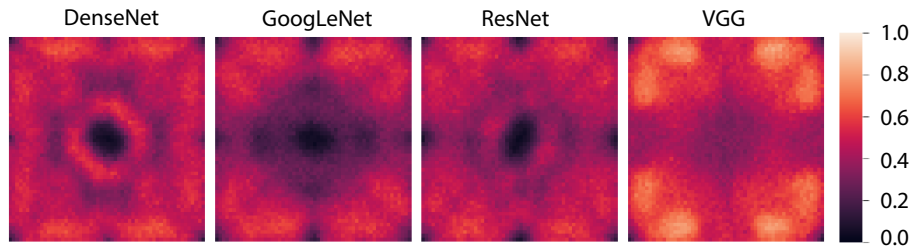


Figure 5: Visualization of sensitivity in the Fourier domain. Visualization procedure is the same with Figure 4.

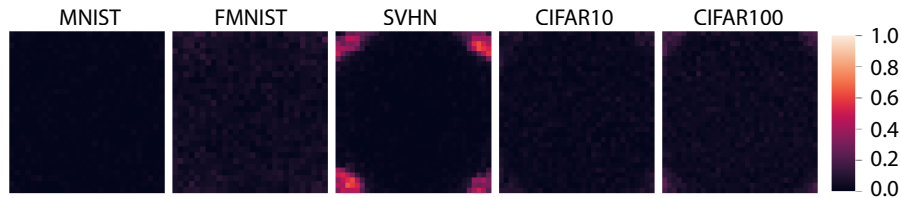


Figure 6: Visualization of the sensitivity of multilayer perceptrons (MLPs) in the Fourier domain. MLPs are resistant to directions of Fourier basis.

the Fourier domain, and effectiveness of characterization by Fourier basis.

5.3 Convolutional networks vs. MLP

We could see that various network architectures on several datasets are sensitive to some Fourier basis in Sec. 5.2. To see whether the sensitivity to the Fourier basis functions is caused by network architectures as suggested in Sec. 4 or the nature of image processing, we compared the sensitivity of convolutional networks and MLP to Fourier basis functions. We used the same method with Sec. 5.2 for the comparison. Figure 6 shows the results for the MLP trained on various datasets. The MLP did not show vulnerability to some vectors in the Fourier basis. The contrastive activation pattern of convolutional networks and multilayer perceptrons supports our analysis of the sensitivity provided in Sec. 4. This result suggests the possibility that changing architectures is a useful measure against adversarial examples, especially against universal ones. Since prior defense work has mostly focused on training methods [6, 19], this opens another research direction for defense methods. For example, we may use the information about weakness in the Fourier domain to choose which models to combine for an ensemble.

5.4 Co-occurrence of sensitivity

In the evaluation in Sec. 5.2 and Sec. 5.3, we observed that convolutional networks showed similar sensitivity to the Fourier basis with similar frequencies. Since Sec. 4 does not cover this phenomenon, we explain it here. In convolutional networks, the

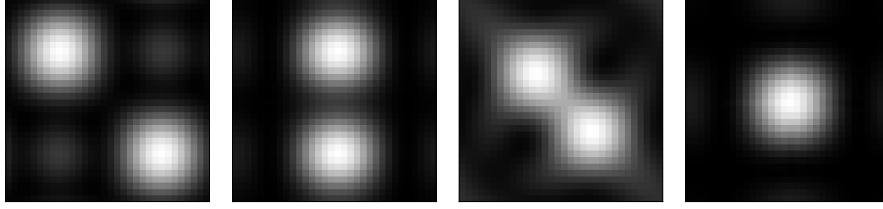


Figure 7: Coordinate (i, j) of each image shows the magnitude of outputs of a convolutional layer when input was $(F_{32})_i \otimes (F_{32})_j$. The kernel size of each convolutional layer is 3. They were trained to maximize the output against $(F_{32})_8 \otimes (F_{32})_8$, $(F_{32})_8 \otimes (F_{32})_{16}$, $(F_{32})_{12} \otimes (F_{32})_{12}$, and $(F_{32})_{16} \otimes (F_{32})_{16}$, respectively.

convolution kernel size is typically much smaller than the input size. The size of the kernel restricts the expressiveness of convolutional layers. This restriction makes convolutional layers respond similarly to similar frequencies. To see the co-occurrence of the sensitivity, we trained a convolutional layer with kernel size 3×3 and the input size 32×32 so that the ℓ_2 -norm of its output become maximized when one specific Fourier basis is fed as its input. Figure 7 shows the result. The result confirms the hypothesis that convolutional layers respond similarly to Fourier basis directions with similar frequency. Thus, practically, we do not have to check sensitivity of each frequency to find the sensitive spots in the Fourier domain.

5.5 UAPs in Fourier domain

In this sections we see whether existing UAPs also have some specific patterns in the Fourier domain. For this analysis, we used precomputed UAPs for VGG16, VGG19, VGG-F, CaffeNet [12], ResNet152, and GoogLeNet by Moosavi-Dezfooli et al. [24]. Figure 8 shows the magnitude of each frequency of each UAP in log scale. For reference, Figure 8 also shows those of random noise and average magnitudes of each frequency of original training data in ILSVRC2015. While architectures and training procedures differ, Figure 8 and Figure 5 share a similar tendency compared to random noise and original images. For example, we can see from Figure 5 that the networks are relatively robust against high-frequency noise and sensitive to low-frequency and middle-frequency noise. From Figure 8, current UAPs exploit this sensitivity. This suggests an effectiveness to consider Fourier domain to analyze existing UAPs.

5.6 Adversarial attacks in Fourier domain

In this section, we see whether current white box adversarial attacks also have some tendency in the Fourier domain. We studied FGSM [6], which is known to transfer better than naive iterative attacks [19]. Figure 9 shows the average magnitude of each vector in Fourier basis of a perturbation created by FGSM on test data. Compared with Figure 4, which revealed sensitive spots in the Fourier domain, Figure 9 shows that the mass of FGSM concentrates almost in the sensitive spots. This experiment also

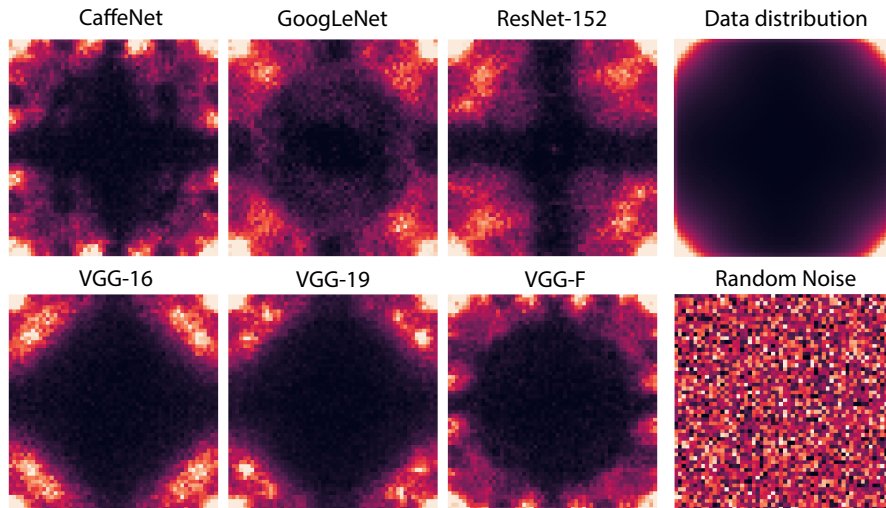


Figure 8: Visualization of UAPs calculated for various architectures on ILSVRC2012 by Moosavi-Dezfooli et al. [24] in the Fourier domain. Coordinate (i, j) corresponds to $(F_{224})_i \otimes (F_{224})_j$. White spots had larger values.

shows that adversarial perturbations do not necessarily lie in a high-frequency area, which denies a common myth that adversarial perturbations tend to be high-frequency. Figure 9 also shows that the tendency of adversarial perturbations differ across datasets and architectures, which reminds us to test defense methods in various settings.

5.7 Effectiveness of Fourier attack

The analysis in Sec. 4 and experiments in Sec. 5.2 – Sec. 5.6 suggests the effectiveness of the Fourier basis functions as universal adversarial perturbations. We evaluated its ability to change predictions on various datasets and architectures. We set the size of perturbations to $10/255$ in ℓ_∞ for CIFAR, and to $30/255$ for MNIST, FMNIST, and SVHN. We used frequencies with highest fool ratio in Figure 4 as the perturbations. In the evaluation, we used Algorithm 1 with one fixed frequency per pair of dataset and architecture. For comparison, we calculated the fool ratio of random noise sampled from the ϵ -ball bounded in ℓ_∞ -norm. Table 1 shows the result. Given the dataset and architecture-agnostic search space, the attack was surprisingly effective. Especially in CIFAR10 and CIFAR100 experiments, some architectures dropped prediction accuracy almost to that of random guessing. This effectiveness of Fourier basis attack highlights the sensitivity of current convolutional networks against Fourier features. We also tested Algorithm 1 on ILSVRC2015. For the evaluation, we fixed one frequency for all architectures and inputs. In other words, we used a single perturbation for both input and architecture agnostically. To choose the frequency, we took the average of Figure 5 and picked the frequency with the highest fool ratio. Figure 1 shows the examples of created adversarial examples. We used $10/255$ and $20/255$ for the size of

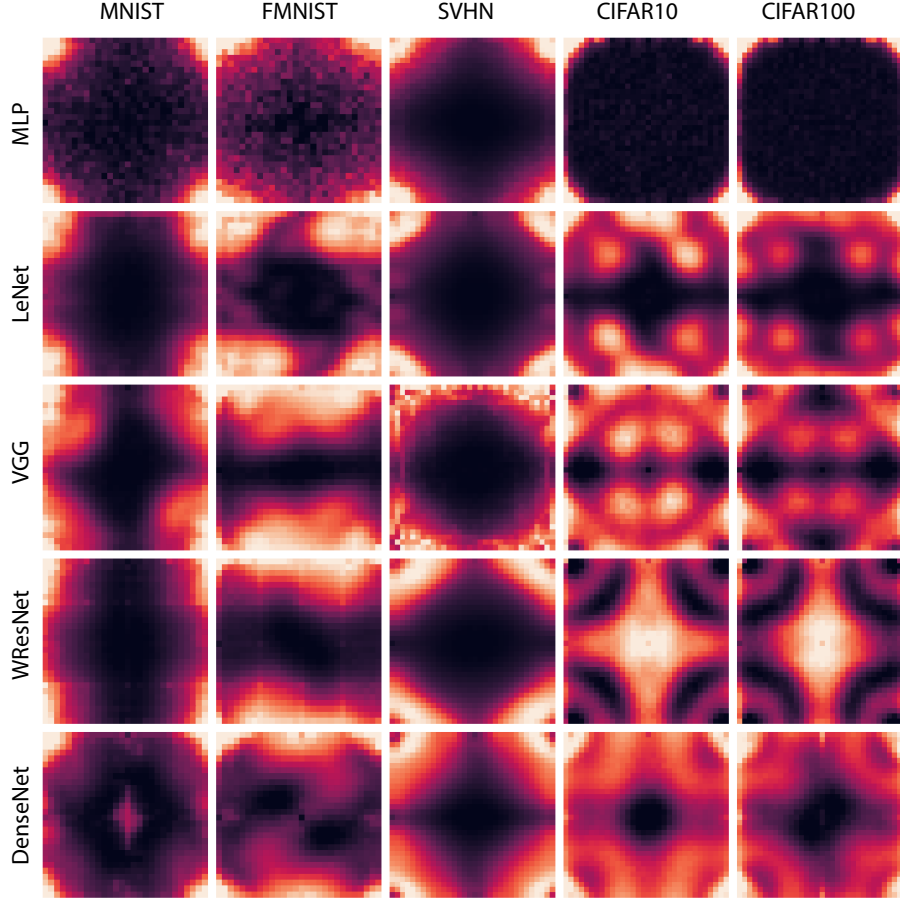


Figure 9: Visualization of FGSM attack in the Fourier domain in the same way as in Figure 8. FGSM had larger values in sensitive spots revealed in Figure 4. Center of each image is a high-frequency area.

perturbations. Note that previous work used $10/255$ for the evaluation [24]. Examples of created UAPs are shown in Figure 1. We empirically found that taking the sign of Fourier basis can sometimes boost the performance of the attack. We named this attack Signed-SFA (SSFA), and we also tested the attack. The result is shown in Table 2. Compared to Moosavi-Dezfooli et al. [24], the fool ratio is comparable to or better than their perturbations in an architecture-agnostic setting. We also note that our algorithm is significantly faster compared to the original UAP algorithm even if we take into account the time needed to find the weak spot. Moreover, our algorithm does not require calculation of gradients nor logits of targets. This enable us to create UAPs in black-box settings, which is contrastive to previous UAPs creation algorithms, which are typically for white-box. Thus, our method is more suitable for practical attack

Table 1: Fool ratio of random noise (upper rows) and SFA (Algorithm 1, lower rows) on various architectures and datasets.

	LeNet	WResNet	VGG	DenseNet
MNIST	0.1	55.8	0.0	0.1
Fashion MNIST	5.4	11.4	8.3	12.6
SVHN	3.1	5.2	0.0	4.6
CIFAR10	5.0	8.1	6.8	5.4
CIFAR100	13.0	26.4	25.9	22.5
MNIST	0.4	90.2	0.1	0.2
Fashion MNIST	12.5	48.1	83.7	56.9
SVHN	64.9	90.8	0.0	50.5
CIFAR10	63.3	82.3	72.2	50.7
CIFAR100	83.4	93.7	95.8	72.3

Table 2: Fool ratio of Fourier basis attack on various architectures on ILSVRC2015. Rand is random noise, SSFA is defined in Sec. 5.7. Attacks are bounded in $10/255$ and $20/255$ in ℓ_∞ -norm.

	GoogLeNet	ResNet	VGG	DenseNet
Rand(10)	8.2	8.5	11.5	9.5
Rand(20)	14.9	16.1	19.7	16.7
SFA(10)	34.6	38.7	49.7	36.8
SFA(20)	62.3	68.5	76.3	63.5
SSFA(10)	44.1	40.1	53.3	39.5
SSFA(20)	74.1	66.9	79.0	62.5

senarios.

6 Conclusion

Starting from a linear hypothesis and the fact that linearized convolutional networks are sensitive to a combination of a few Fourier basis functions, we investigated the sensitivity of convolutional networks in the Fourier domain. Through empirical evaluations, we figured out that the current high-performance deep convolutional networks are vulnerable in Fourier basis directions. Empirical findings also suggest that current adversarial attacks also exploits the vulnerability in the Fourier domain to some extent. As a by-product of the analysis, we proposed an efficient black-box method to create universal adversarial perturbations. We believe that this work will be a pivotal milestone in understanding and mitigating the sensitivity of convolutional networks to input

noises.

7 Acknowledgments

YT was supported by Toyota/Dwango AI scholarship. IS was supported by KAKEN 17H04693.

References

- [1] N. Ahmed, T. Natarajan, and K. R. Rao. Discrete Cosine Transform. *IEEE Transactions on Computers*, pages 90–93, 1974.
- [2] A. Athalye, N. Carlini, and D. Wagner. Obfuscated Gradients Give a False Sense of Security: Circumventing Defenses to Adversarial Examples. In *Proceedings of the 35th International Conference on Machine Learning*, pages 274–283, 2018.
- [3] N. Carlini and D. A. Wagner. Towards Evaluating the Robustness of Neural Networks. In *Proceedings of the 2017 IEEE Symposium on Security and Privacy*, pages 39–57. IEEE Computer Society, 2017.
- [4] J. W. Cooley and J. W. Tukey. An Algorithm for the Machine Calculation of Complex Fourier Series. *Mathematics of Computation*, pages 297–301, 1965.
- [5] I. Goodfellow, Y. Bengio, and A. Courville. *Deep Learning*. MIT Press, 2016. <http://www.deeplearningbook.org>.
- [6] I. J. Goodfellow, J. Shlens, and C. Szegedy. Explaining and Harnessing Adversarial Examples. *International Conference on Learning Representations*, 2015.
- [7] P. Goyal, P. Dollár, R. Girshick, P. Noordhuis, L. Wesolowski, A. Kyrola, A. Tulloch, Y. Jia, and K. He. Accurate, Large Minibatch SGD: Training ImageNet in 1 Hour. *CoRR*, abs/1706.02677, 2017.
- [8] C. Guo, M. Rana, M. Cisse, and L. v. d. Maaten. Countering Adversarial Images using Input Transformations. *International Conference on Learning Representations*, 2018.
- [9] K. He, X. Zhang, S. Ren, and J. Sun. Deep Residual Learning for Image Recognition. In *The IEEE Conference on Computer Vision and Pattern Recognition*, pages 770–778, 2016.
- [10] G. Huang, Z. Liu, L. van der Maaten, and K. Q. Weinberger. Densely Connected Convolutional Networks. In *The IEEE Conference on Computer Vision and Pattern Recognition*, pages 2261–2269, 2017.
- [11] A. K. Jain. *Fundamentals of digital image processing*. Prentice-Hall, Inc., 1989.

- [12] Y. Jia, E. Shelhamer, J. Donahue, S. Karayev, J. Long, R. Girshick, S. Guadarrama, and T. Darrell. Caffe: Convolutional architecture for fast feature embedding. In *ACM International Conference on Multimedia*, page 675678, 2014.
- [13] J. Jo and Y. Bengio. Measuring the tendency of CNNs to Learn Surface Statistical Regularities. *CoRR*, abs/1711.11561, 2017.
- [14] G. Karolina Dziugaite, Z. Ghahramani, and D. M. Roy. A study of the effect of JPG compression on adversarial images. *CoRR*, abs/1608.00853, 2016.
- [15] V. Khrulkov and I. Oseledets. Art of singular vectors and universal adversarial perturbations. *CoRR*, 2017.
- [16] J. Z. Kolter and E. Wong. Provable Defenses against Adversarial Examples via the Convex Outer Adversarial Polytope. In *Proceedings of the 35th International Conference on Machine Learning*, pages 5286–5295, 2018.
- [17] A. Krizhevsky. Learning Multiple Layers of Features from Tiny Images. 2009.
- [18] A. Krizhevsky, I. Sutskever, and G. E. Hinton. ImageNet Classification with Deep Convolutional Neural Networks. In *Advances in Neural Information Processing Systems 25*, pages 1097–1105, 2012.
- [19] A. Kurakin, I. J. Goodfellow, and S. Bengio. Adversarial Machine Learning at Scale. *International Conference on Learning Representations*, 2017.
- [20] Y. Lecun, L. Bottou, Y. Bengio, and P. Haffner. Gradient-based Learning Applied to Document Recognition. In *Proceedings of the IEEE*, pages 2278–2324, 1998.
- [21] Y. LeCun, C. Cortes, and C. J. C. Burges. The MNIST Database of Handwritten Digits, 1998. URL <http://yann.lecun.com/exdb/mnist/>.
- [22] Y. Liu, X. Chen, C. Liu, and D. Song. Delving into Transferable Adversarial Examples and Black-box Attacks. *International Conference on Learning Representations*, 2017.
- [23] S. Moosavi-Dezfooli, A. Fawzi, and P. Frossard. DeepFool: A Simple and Accurate Method to Fool Deep Neural Networks. In *Proceedings of the IEEE Conference on Computer Vision and Pattern Recognition*, pages 2574–2582, 2016.
- [24] S. Moosavi-Dezfooli, A. Fawzi, O. Fawzi, and P. Frossard. Universal adversarial perturbations. In *Proceedings of the IEEE Conference on Computer Vision and Pattern Recognition*, pages 1765–1773, 2017.
- [25] S. Moosavi-Dezfooli, A. Fawzi, O. Fawzi, P. Frossard, and S. Soatto. Robustness of Classifiers to Universal Perturbations: A Geometric Perspective. *International Conference on Learning Representations*, 2018.
- [26] K. R. Mopuri, U. Garg, and R. V. Babu. Fast Feature Fool: A data independent approach to universal adversarial perturbations. In *Proceedings of the British Machine Vision Conference*, 2017.

- [27] Y. Netzer, T. Wang, A. Coates, A. Bissacco, B. Wu, and A. Y. Ng. Reading Digits in Natural Images with Unsupervised Feature Learning. *Neural Information Processing Systems Workshop*, 2011.
- [28] N. Papernot, P. McDaniel, and I. J. Goodfellow. Transferability in Machine Learning: from Phenomena to Black-Box Attacks using Adversarial Samples. *CoRR*, abs/1605.07277, 2016.
- [29] O. Russakovsky, J. Deng, H. Su, J. Krause, S. Satheesh, S. Ma, Z. Huang, A. Karpathy, A. Khosla, M. Bernstein, A. C. Berg, and L. Fei-Fei. ImageNet Large Scale Visual Recognition Challenge. *International Journal of Computer Vision (IJCV)*, pages 211–252, 2015.
- [30] H. Sedghi, V. Gupta, and P. M. Long. The Singular Values of Convolutional Layers. *CoRR*, abs/1805.10408, 2018.
- [31] K. Simonyan and A. Zisserman. Very deep convolutional networks for large-scale image recognition. *CoRR*, abs/1409.1556, 2014.
- [32] S. Song, Y. Chen, N.-M. Cheung, and C.-C. J. Kuo. Defense Against Adversarial Attacks with Saak Transform. *CoRR*, abs/1808.01785, 2018.
- [33] C. Szegedy, W. Zaremba, I. Sutskever, J. Bruna, D. Erhan, I. J. Goodfellow, and R. Fergus. Intriguing Properties of Neural Networks. *International Conference on Learning Representations*, 2014.
- [34] C. Szegedy, W. Liu, Y. Jia, P. Sermanet, S. Reed, D. Anguelov, D. Erhan, V. Vanhoucke, and A. Rabinovich. Going Deeper with Convolutions. In *The IEEE Conference on Computer Vision and Pattern Recognition*, 2015.
- [35] F. Tramèr, N. Papernot, I. J. Goodfellow, D. Boneh, and P. D. McDaniel. The Space of Transferable Adversarial Examples. *CoRR*, abs/1704.03453, 2017.
- [36] F. Tramèr, A. Kurakin, N. Papernot, D. Boneh, and P. D. McDaniel. Ensemble Adversarial Training: Attacks and Defenses. *International Conference on Learning Representations*, 2018.
- [37] J. Uesato, B. ODonoghue, P. Kohli, and A. Oord. Adversarial Risk and the Dangers of Evaluating Against Weak Attacks. In *Proceedings of the 35th International Conference on Machine Learning*, pages 5025–5034, 2018.
- [38] L. Weng, H. Zhang, H. Chen, Z. Song, C. Hsieh, L. Daniel, D. Boning, and I. Dhillon. Towards Fast Computation of Certified Robustness for ReLU Networks. In *Proceedings of the 35th International Conference on Machine Learning*, pages 5276–5285, 2018.
- [39] H. Xiao, K. Rasul, and R. Vollgraf. Fashion-MNIST: a Novel Image Dataset for Benchmarking Machine Learning Algorithms. *CoRR*, abs/1708.07747, 2017.
- [40] S. Zagoruyko and N. Komodakis. Wide Residual Networks. In *Proceedings of the British Machine Vision Conference*, pages 87.1–87.12, 2016.